Journal of Applied Electrochemistry **30**: 865–874, 2000.

Studies on the influence of chloride ion and pH on the corrosion and electrochemical behaviour of AZ91D magnesium alloy

R. AMBAT, N.N. AUNG and W. ZHOU
School of Mechanical and Production Engineering, Nanyang Technological University, Nanyang Avenue, Singapore 639798

Received 12 October 1999; accepted in revised form 20 January 2000

Key words: AZ91D alloy, chloride ion, corrosion, die-cast, ingot, magnesium alloys, pH

Abstract

The influence of chloride ion concentration and pH on the corrosion and electrochemical behaviour of die-cast and ingot-cast AZ91D alloy have been studied with a focus on the stability of microconstituents in these environments. The experimental techniques used include immersion studies, potentiodynamic polarization, X-ray diffraction and optical and scanning electron microscopy. The corrosion rate for the ingot and die-cast was very high in highly acidic solutions (pH 1–2) as compared to that in neutral and highly alkaline solutions (pH 4.5–12.0), and the rate increased with chloride ion concentration at all pH levels. In general, the die-cast showed a lower corrosion rate at all pH values and chloride ion concentrations. The open circuit corrosion potential shifted to more negative (more active) values with increase in concentration of chloride ions. Corrosion morphologies revealed more attack on primary α and eutectic α with increasing chloride concentration. In highly acidic conditions, corrosion attack was found on β ($Mg_{17}Al_{12}$) and eutectic α phase (α regions with higher Al content) while at pH 12.0 the ingot exhibited a pitting type of morphology. The corrosion product consisted of magnesium hydroxide, fallen β particles and magnesium–aluminium oxide; the amount of each component was found to be a function of chloride ion concentration and pH.

1. Introduction

Because of their low density, high specific strength and stiffness, magnesium alloys have become candidate materials for many applications in microelectronics and in the automobile and aerospace industries. The relative density of magnesium is 1.74, that is 35% lower than that of aluminium, and typical magnesium alloys weigh ~35% lower than their aluminium counterparts at equal stiffness [1]. In addition, these alloys have good castability and damping capacity.

The magnesium–aluminum system has been the basis of the most widely used magnesium casting alloys since these materials were introduced in Germany during the First World War [2]. Most of these alloys contain 8–9% aluminum with small amounts of zinc. Among these the AZ91 series alloys have found widespread applications in the automotive industry.

A serious limitation for the potential use of several magnesium alloys, and AZ91 in particular, is their susceptibility to corrosion. Magnesium alloys, especially those with high purity, have good resistance to atmospheric corrosion. However, the susceptibility to corrosion in chloride containing environments is a serious concern. The standard electrochemical potential of magnesium is −2.4 V vs NHE, even though in aqueous solutions it shows a potential of −1.5 V due to the formation of $Mg(OH)_2$ film [1]. Consequently, magnesium dissolves rapidly in aqueous solutions by evolving hydrogen below pH 11.0, the equilibrium pH value for $Mg(OH)_2$ [1].

The general corrosion and electrochemical behaviour of AZ91 series alloys have been studied [3–7]. The majority of these studies have focused on the effect of processing route and microstructure. To date, there has been no detailed study on the effect of pH and chloride ion concentration on the corrosion behaviour of cast AZ91 magnesium alloy. In AZ91, magnesium and the principal alloying element aluminium, have distinct E_h–pH stability domains, so that the effect of chloride ions and pH may differ depending on this stability pattern. Hence, the AZ91 microstructure consisting of β phase, eutectic α and primary α and change in morphology of these phases resulting from the processing route could behave differently under varying pH conditions and chloride concentrations. It is important to understand the effect of these parameters in detail on all microconstituents in the microstructure of the alloy. The present investigation was aimed at investigating these aspects in AZ91D alloy prepared by ingot casting and die-casting.

2. Experimental details

2.1. *Material*

The AZ91D die-cast material (die-cast) was available in cylindrical rod form with a diameter of about 10 mm. Circular specimens of thickness 2 mm were sliced from the rod. For ingot material (ingot), a specimen size of 1 cm × 1 cm × 2 mm was used for the experiments. The chemical composition of the alloy is given in Table 1.

2.2. *Corrosive media*

The effect of chloride ion concentration was studied in solutions containing various amounts of NaCl (0–10%) at pH 7.25. For study of the effect of pH, the chloride ion concentration was kept constant at 3.5% while the pH was varied from 1–12.0. All the experiments were conducted at room temperature. The solution was prepared using AR grade NaCl in distilled water. The pH of the solution was adjusted with HCl/NaOH.

2.3. *Immersion testing*

For immersion testing, the specimens were polished successively on finer grades of emery papers up to 1000 level. All the specimens were initially cleaned following the procedure of ASTM standard G-I-72 [8]. The polished and preweighed specimens were exposed to the solution (150 ml) for various times. At the end of the experiment, cleaning of the specimens was carried out by dipping in a solution of 15% CrO_3 + 1% $AgCrO_4$ in 100 ml of water under boiling conditions. An acetone wash followed this. The weight loss was measured after each experiment and the corrosion rate was calculated in millimetres per year. In each case duplicate experiments were conducted, the results were found to fall within the expected error.

2.4. *Electrochemical testing*

Electrochemical polarization experiments were carried out using an Auto Lab Corrosion measurement system. Electrodes for this purpose were prepared by connecting a wire to one side of the sample that was covered with cold setting resin. The opposite surface of the specimen was exposed to the solution. The exposed area was about 1 cm^2. The specimens were given a metallographic polishing prior to each experiment, followed by washing with distilled water and acetone. Polarization measurements were carried out in a corrosion cell containing 150 ml of the solution using a standard three-electrode configuration: saturated calomel was used as reference with a platinum electrode as counter. Specimens were immersed in the test solution and a polarization scan was carried out towards more noble values at a rate of 1 mV s^{-1}, after allowing a steady state potential to develop.

Table 1. Chemical composition of the AZ91D alloy (in wt%)

Al	Mn	Ni	Cu	Zn	Ca	Si	K	Fe	Mg
9.1	0.17	0.001	0.001	0.64	< 0.01	< 0.01	< 0.01	< 0.001	Bal

2.5. *Surface morphology and corrosion product analysis*

The microstructure and surface morphology of the corroded surfaces were characterised using the optical (Zeiss model) and scanning electron microscope (Jeol, model 5600LV).

X-ray diffraction technique (Philips, model PW1830) was used for the analysis of the corrosion product. The corrosion product was collected by filtration of the corrosive media and washed with water to remove sodium chloride. The product was dried before subjecting to X-ray analysis. All the experiments were carried out at room temperature (30 °C) and the solution as gently stirred during the experiment. For experiments with a starting pH 2.0 and 7.25, the pH of the solution increased with time of exposure due to magnesium dissolution to a final pH value of 9.0 and 9.58. All the experiments were continued for five days before collecting the product for analysis.

3. Results

3.1. *Microstructure*

Figure 1 shows microstructure of the die-cast and ingot. The microstructure consisted of primary α, eutectic α and β phases (marked in the Figure). Die-cast showed much finer grains and β phases. Considerable porosity was observed on the die-cast. On the other hand, the ingot showed coarse grain structure with longer β particles.

Coring during solidification causes considerable variation in the distribution of aluminium and zinc in the microstructure of AZ91D alloy and is found to have significant influence on corrosion behaviour [9]. Figure 2 gives typical concentration profiles of aluminium and zinc in AZ91D alloy along the lines shown in the micrographs measured using EDX. In general, the aluminium and zinc concentration at α regions near to β phase (eutectic α) was high (non-corroded region), and decreased with increase in distance from the β phase. The width of this aluminium rich region (>8%) adjacent to the β phase varied at different sites. The concentration of aluminium typically varied between ~35% at the β phase to about ~8–6% near or with in the primary α phase (corroded region). In the case of die-cast, a similar feature was observed, except that the width of β phase and eutectic α regions was comparatively small.

3.2. *Influence of chloride ion concentration and pH*

3.2.1. *Corrosion rate*

Figure 3 shows the corrosion rate as a function of chloride ion concentration for AZ91D die-cast and ingot

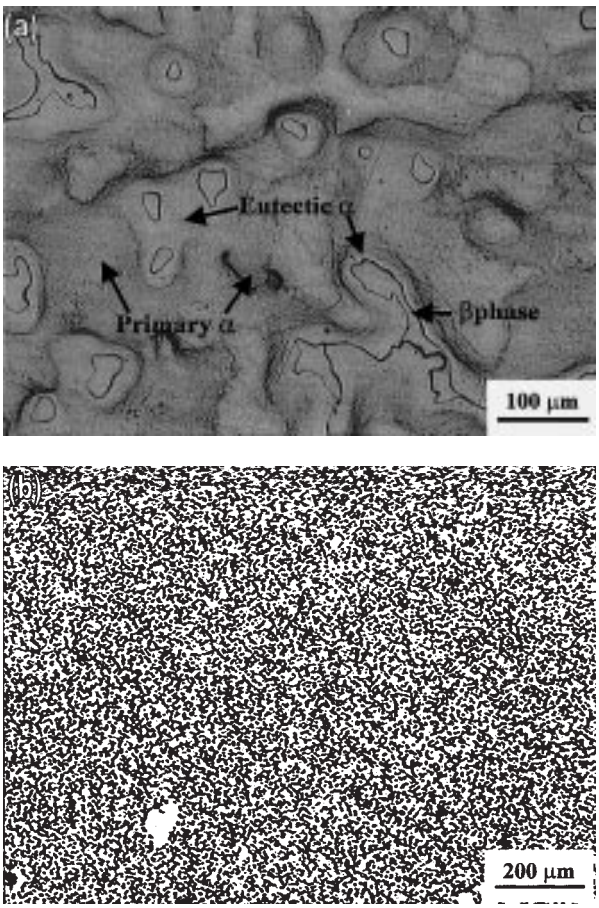

Fig. 1. Microstructures of AZ91D alloy (a) ingot and (b) die-cast.

at three pH values. Both materials exhibited a rise in corrosion rate with increase in chloride ion concentration at pH 7.25 and 12.0 while at pH 2.0 a negligible influence of chloride ion concentration was found. Ingot showed a 10 fold increase in corrosion rate for an increase in chloride ion concentration from 0% to 10% at pH 7.25 and the influence was much higher at pH 12.0. Figure 3 indicates considerable difference in corrosion rates at pH 7.25 obtained from immersion studies and electrochemical measurements. In general die-cast showed lower corrosion rate at all chloride ion concentrations, more significantly at pH 12.0.

Figure 4 shows the corrosion rate against pH for die-cast and ingot in 3.5% NaCl solution. Both materials exhibited a decrease in corrosion rate with increase in pH. Highest corrosion rate was observed at pH 1.0 and a decrease of one unit of pH had decreased the corrosion rate tenfold. In the neutral pH region, the corrosion rate remained constant for both materials and a comparatively low corrosion rate was observed in alkaline solutions. At all pH conditions, die-cast showed lower corrosion rate compared to ingot.

3.2.2. *Potentiodynamic polarization*

The potentiodynamic polarisation curves for the ingot and die-cast in different chloride concentrations are given in Figure 5. No passivity was observed in any of the solutions. The intersecting point of the anodic and cathodic curve (E_{corr}) did not show a significant shift with increase in chloride ion concentration up to 5 wt%, but for 10 wt% NaCl a large negative shift (towards active side) was observed. The magnitude of this negative shift was much higher for ingot. The cathodic curve for die-cast shifted to higher current density values with increase in chloride ion concentration (except for 3.5% NaCl) while a similar shift was not observed for ingot. The anodic curve for both materials also revealed a shift to higher current density values with increase in chloride ion concentration.

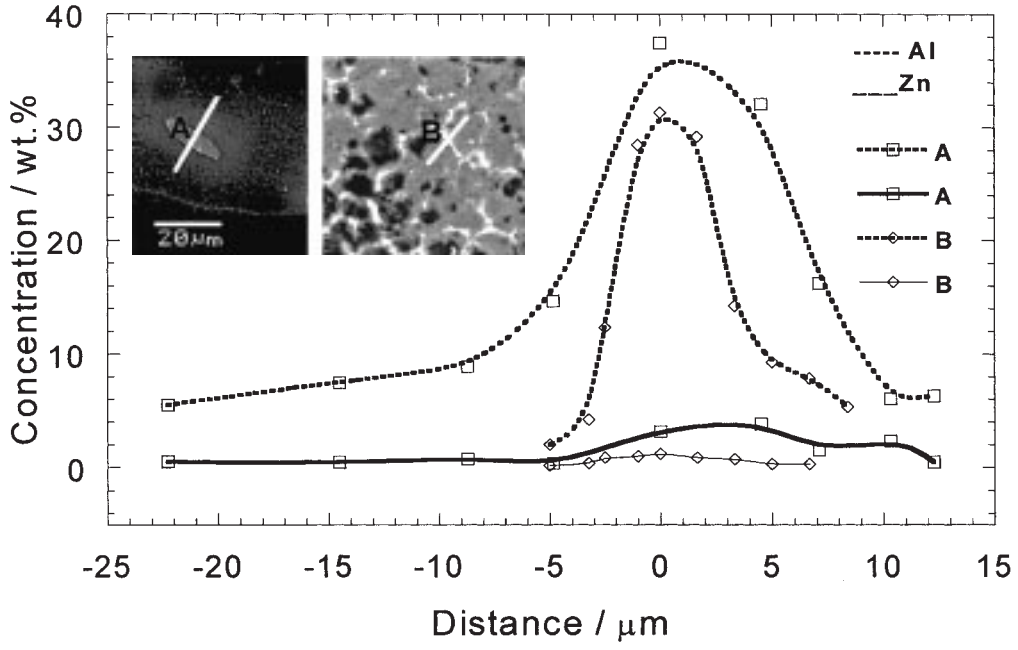

Fig. 2. Concentration profiles for Al and Zn along the line shown in the micrographs for AZ91D alloy: (A) ingot and (B) die-cast.

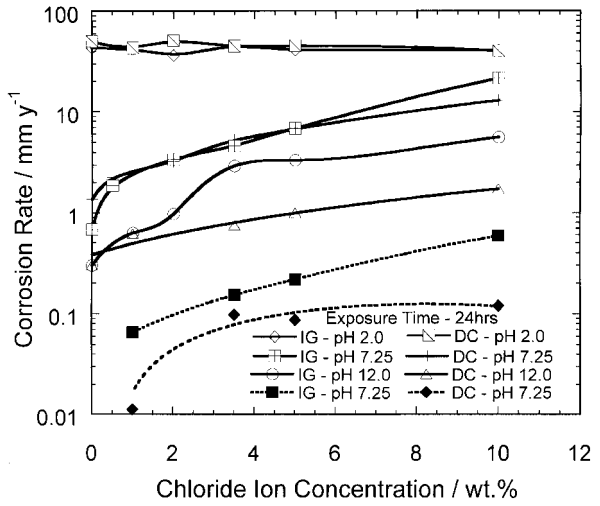

Fig. 3. Corrosion rate for AZ91D ingot and die-cast as a function of chloride ion concentration (dashed lines indicate corrosion rate calculated from electrochemical measurements). Exposure time 24 h.

Figure 6 shows the potentiodynamic polarization curves for ingot and die-cast at different pH conditions. The curves showed no passivity and a more negative (more active) E_{corr} at pH 2.0 that shifted to a less negative (less active) value at pH 7.25 and back to a more negative (more active) value at pH 12.0. The cathodic and anodic current density at all potentials was much higher at pH 2.0 for ingot. For die-cast, the cathodic current density showed no appreciable change with change of pH from 2.0 to 7.25. However, at pH 12.0, the cathodic current density was much lower for both ingot and die-cast. The lowest anodic current density was observed at pH 7.25 for both materials, although the anodic curve of die-cast at pH 12.0 crossed the one at pH 7.25 at higher potentials to show lower current values.

Tables 2 and 3 gives various electrochemical parameters derived from the polarisation curves at different chloride ion concentrations and pH. The open circuit corrosion potential (OCP) values were measured after 30 min. of immersion of the sample. In general, for ingot and die-cast, OCP shifted to more negative values (more active) with increase in chloride ion concentration. Among the three pH conditions evaluated, the OCP was more negative (more active) at pH 2.0 and pH 12.0 compared to that at pH 7.25. The corrosion rate (calculated from I_{corr} values) was higher at pH 2.0 condition, however in contrast to immersion studies, the lowest corrosion rate was observed at pH 7.25. Also, the corrosion rates from electrochemical studies were much lower than that from immersion studies. At all chloride ion concentration and pH values, the β_c values varied between 0.15–0.26 V (decade)$^{-1}$.

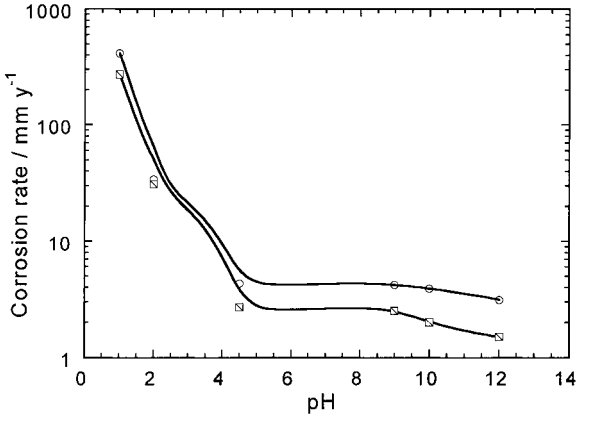

Fig. 4. Corrosion rates for AZ91D ingot and die-cast as a function of pH. Key: (○) AZ91 ingot; (▨) AZ91 die-cast. 3.5% NaCl; exposure time 6 h.

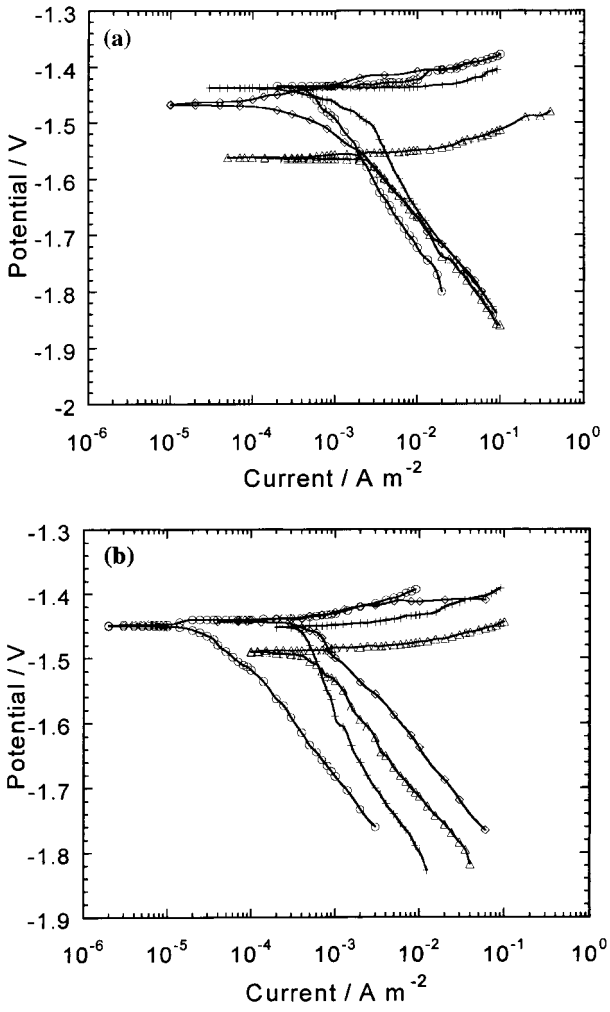

Fig. 5. Potentiodynamic polarization curves for AZ91D alloy as a function of chloride ion concentration at pH 7.25 (a) ingot and (b) die-cast. Scan rate 1 mV s^{-1}. Key: (○) 1%, (◇) 3.5%, (–) 5% and (△) 10%.

3.2.3. *Surface Morphology*

Figures 7 and 8 show the typical surface features of the corroded surfaces of ingot and die-cast exposed to different chloride concentrations. For die-cast, the pictures were taken on samples exposed to the corrosive media for 15 min, as it was difficult to reveal the corrosion features on 24 h exposed ones. The pictures shown in Figure 8 were recorded in back scattered mode to obtain better clarity. The extent of attack increased

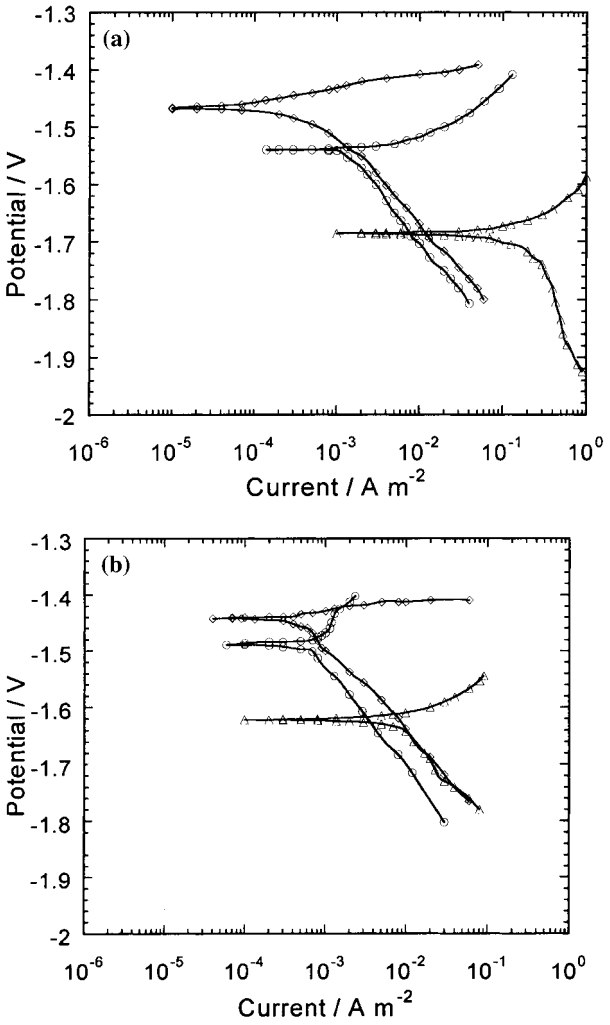

Fig. 6. Potentiodynamic polarization curves for AZ91D alloy at various pH conditions (a) ingot and (b) die-cast. 3.5% NaCl. Scan rate 1 mV s^{-1}. Key: (△) pH 2.0, (◇) pH 7.25, (○) pH 12.0.

both on ingot and die-cast with increasing chloride ion concentration. More interestingly, a closer looks at the micrographs (Figures 7 and 8) reveals that the corrosion characteristics of various microconstituents changed with change in chloride ion concentration. A comparison of the micrographs in Figures 7 and 8 with Figure 2 reveals that at low chloride concentrations, the corrosion attack was concentrated primarily on regions with low aluminium (primary α) while at 10% NaCl corrosion attack spread to the regions with higher concentrations of aluminium (eutectic α) and to the β/α boundaries at several locations. For die-cast severe pitting can be seen on primary α phase.

Figures 9 and 10 show typical photomicrographs of the corroded surface at different pH values. As mentioned previously, the pictures for die-cast was taken on samples exposed for 15 min and in the back scattered mode. The surface topographic pictures are in agreement with corrosion rate measurements. It can be seen that as pH increases towards alkaline side the severity of attack decreases. For ingot, at pH 1.0, the entire surface was attacked. The morphology of the attack changes

Table 2. Electrochemical parameters for AZ91D ingot and die-cast in solution containing increasing concentration of chloride ions

Chloride ion concentration/wt%	Open circuit corrosion potential/V	β_c/V
Ingot		
1	−1.555	0.225
3.5	−1.582	0.168
5	−1.603	0.219
10	−1.618	0.175
Die-cast		
1	−1.566	0.161
3.5	−1.509	0.158
5	−1.576	0.240
10	−1.587	0.167

with increase pH to give a pitting type of corrosion at pH 12.0. For die-cast, aggressive attack can be seen on the surface at pH 1.0 that decreased with increase in pH towards alkaline side. However on both materials, the change in pH had significant effect on the corrosion behaviour of different microconstituents namely β phase, eutectic α and primary α. Analysis of the micrographs in comparison with Figure 2 shows that at pH 2.0, none of microconstituents are stable. Figure 9(a) shows severe attack on other wise stable eutectic α and β phase in ingot. The photographs for die-cast at pH 2.0 (Figure 10(b)) shows channels where β phases were dissolved or undermined (see arrows in Figure 10(b)). However, the pattern at pH 7.25 and 12.0 indicates that the eutectic α and β phases were highly stable under these conditions for ingot while for die-cast at pH 12.0 the picture revealed removal of β phase from the surface either by dissolution or undermining.

3.2.4. *Corrosion product analysis*

X-ray diffractogram of corrosion products for die-cast and ingot in 3.5% and 10% NaCl (Figure 11) exhibited considerable difference in composition of corrosion product. The product for ingot in 3.5% NaCl (Figure 11) consisted mainly of $Mg(OH)_2$, fallen β particles and small amounts of magnesium–aluminium oxides (mixed oxides). The exact composition of these mixed oxides is not clear although the peaks were found to match those reported for the compounds such as $Mg_{0.866}Al_{1.83}O_{3.611}$, $MgAl_2(OH)_8$ H_2O, $Mg_2Al(OH)_{10}$ H_2O and $MgAl(OH)_{14}$ H_2O. Increase in chloride concentration

Table 3. Electrochemical parameters for AZ91D ingot and die-cast in 3.5% NaCl solution of different pH

pH	Open circuit corrosion potential/V	Corrosion rate/mm y^{-1}	β_c/V
Ingot			
2.00	−1.680	0.1500	0.260
7.25	−1.582	0.0005	0.168
12.00	−1.603	0.0010	0.171
Die-cast			
2.00	−1.600	0.00800	0.152
7.25	−1.510	0.00045	0.158
12.00	−1.557	0.00060	0.200

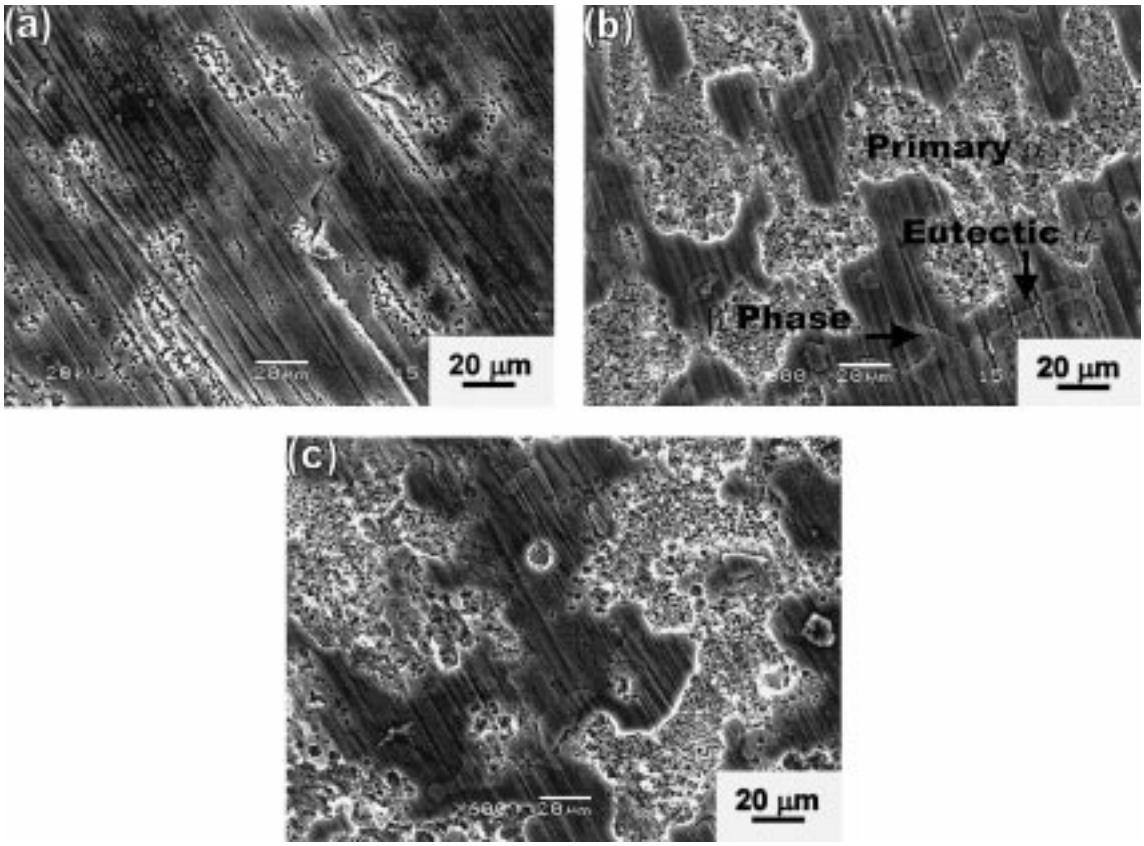

Fig. 7. Scanning electron micrographs for ingot showing effect of chloride ion concentration on corrosion morphology: (a) 0% NaCl, (b) 3.5% NaCl and (c) 10% NaCl.

to 10% increased the relative amount of fallen β particles in the corrosion product simultaneously with an increase in the amount of mixed oxides. Die-cast material exhibited a similar behaviour with a higher amount of mixed oxides at 10% NaCl, although the relative amount of β particles did not change drastically.

X-ray diffractograms of the corrosion product formed in different pH conditions are given in Figure 12. The patterns for ingot did not show much change in corrosion product as a function of pH except that a relatively higher amount of mixed oxides ($Mg_{0.866}Al_{1.83}O_{3.611}$, $MgAl_2(OH)_8$ H_2O, $Mg_2Al(OH)_{10}$ H_2O and $MgAl(OH)_{14}$ H_2O) in pH 2.0 and pH 12.0 conditions was formed. However, $Mg(OH)_2$ was present in large amounts. For die-cast, the influence of pH on corrosion product was more significant. While the product showed considerably lower intensity peaks for β phase at pH 7.25, the patterns at pH 2.0 and 12.0 showed a significant increase of fallen β particles in the product. An equivalent increase in the amount of mixed oxide was also detected from the diffractograms.

4. Discussion

4.1. *General corrosion and electrochemical behaviour*

Corrosion and electrochemical behaviour of ingot and die-cast were significantly influenced by chloride ions and pH. The increase in corrosion rate with increasing chloride ion concentration at pH 7.25 and 12.0 (Figure 3) may be attributed to the participation of chloride ions in the dissolution reaction. Chloride ions are aggressive for both magnesium and aluminium. The adsorption of chloride ions to oxide covered magnesium surface transforms $Mg(OH)_2$ to easily soluble $MgCl_2$. The critical concentration of chloride ions required for pitting of magnesium in uninhibited NaCl was reported to be about 0.002 to 0.02 M NaCl [10]. This value increases with increase in pH of the solution.

In agreement with the above observations, the polarization curves exhibited an increase in anodic current density with increase in chloride ion concentration (Figure 5). In the case of die-cast (Figure 5b) cathodic curve also shifted to higher current density values with increase in chloride ion concentration. The shift of OCP to more negative (more active) values with increase in chloride ion (Table 2) concentration may be explained by the adsorption of these ions on the alloy surface at weak parts of the oxide film [11].

The effect of pH on the corrosion behaviour is in agreement with the Eh–pH diagram [12] of magnesium and aluminium. The dissolution of magnesium in aqueous solutions proceeds by the reduction of water to produce magnesium hydroxide and hydrogen gas. Supporting this, the β_c values given in Tables 2 and 3 indicate that the reduction process was primarily water

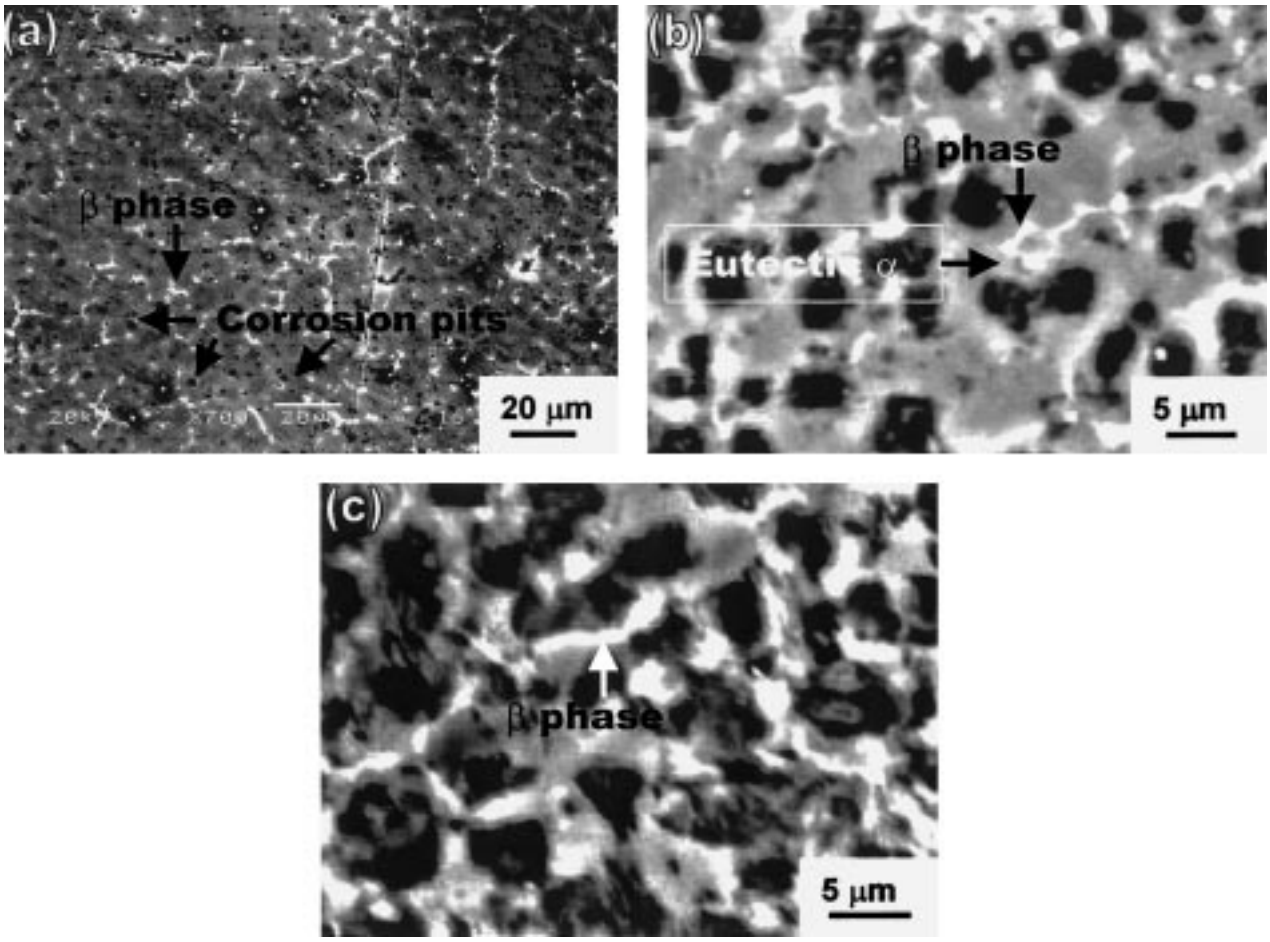

Fig. 8. Scanning electron micrographs (backscattered mode) for die-cast showing effect of chloride ion concentration on corrosion morphology: (a) 0% NaCl, (b) 3.5% NaCl and (c) 10% NaCl.

reduction. These reactions are reported to be insensitive to oxygen concentration [13, 14].

$$Mg \rightarrow Mg^{2+} + 2e^{-} \quad (1)$$

$$2H_2O + 2e^{-} \rightarrow H_2 + 2(OH)^{-} \quad (2)$$

$$Mg^{2+} + 2(OH)^{-} \rightarrow Mg(OH)_2 \quad (3)$$

The equilibrium pH value required for the precipitation of $Mg(OH)_2$is around 11.0.

Highly acidic solutions are aggressive to both magnesium and aluminium, hence a very high corrosion rate (Figure 4). The lower corrosion rate at pH above 4.0 may be due to less aggressiveness of the solution and also as this pH falls in the passive region for aluminium, if not for magnesium. In the pH range ~4–9, aluminium is passive and a pH above ~9.0 favour the formation of magnesium–aluminate and $Mg(OH)_2$ (depending on the concentration of magnesium in solution).

In agreement with the above, the corrosion product showed two types of passivating compounds in the range of pH studied; namely, $Mg(OH)_2$ and a group of magnesium–aluminium oxides (Figures 11 and 12). The latter was present mainly in corrosive media (pH 2.0, 12.0 and 10% NaCl) where the dissolution of aluminium was assumed to be high. Under alkaline conditions these mixed oxides are stable and offer better protection for both materials. In the present study, the formation of mixed oxides or $Mg(OH)_2$ in corrosion media with starting pH 2.0 does not mean that these products are stable at this pH value. As mentioned earlier, for experiments with starting pH 2.0, the final pH value while removing the product (after 5 days) was around 9.0. Hence the precipitation of the compounds might have occurred at higher pH values during the course of the experiment depending on the concentration of magnesium and aluminium in the solution. However, the presence of mixed oxides and β phase in the corrosion product indicate dissolution of more aluminium and electrochemical oxidation or undermining of β phase (as is evident from Figures 9(a) and 10(b)).

The results of electrochemical studies (Figure 6 and Table 3) shows highest corrosion rate, most active OCP and a higher anodic and cathodic current densities, at pH 2.0. It is interesting to observe that the anodic curve for ingot at pH 12.0 (Figure (6a)) showed significantly higher anodic current densities compared to that at pH 7.25, while for die-cast, the anodic curve at pH 12.0 exhibited a passive type behaviour and very low

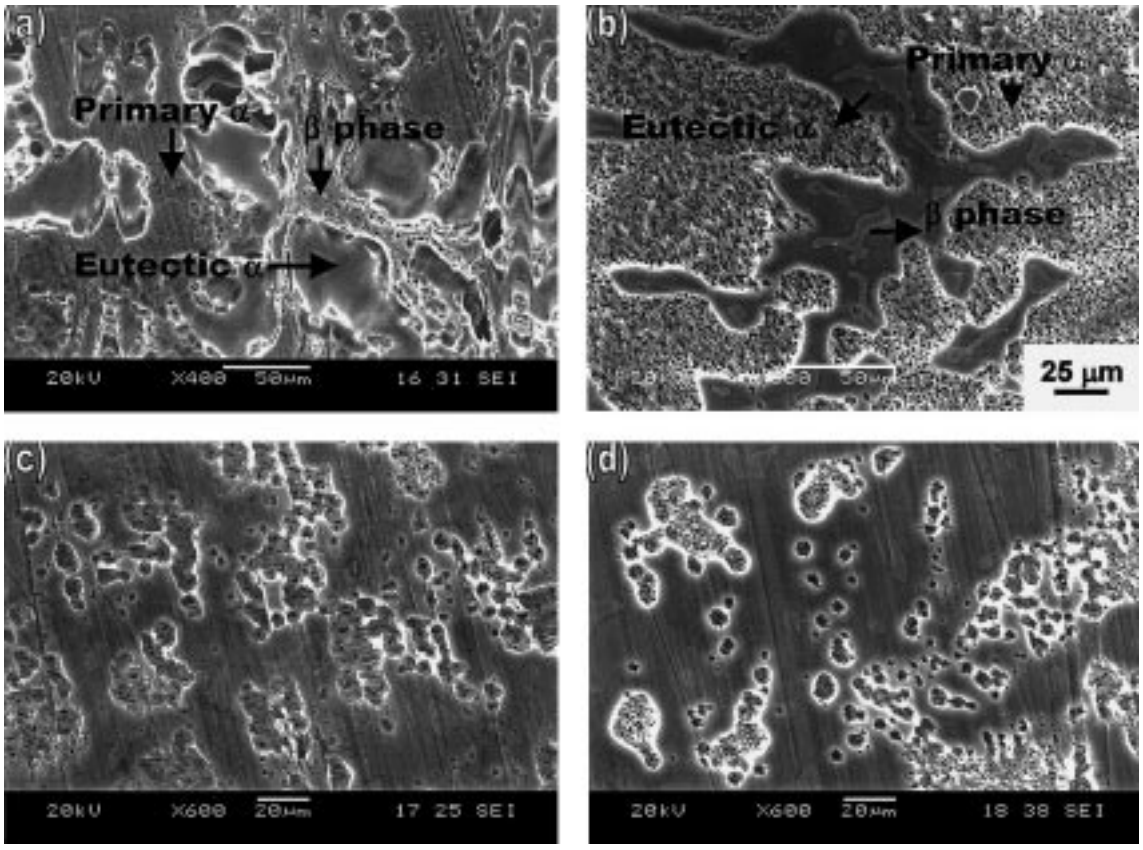

Fig. 9. Scanning electron micrographs for ingot showing effect of pH on corrosion morphology: (a) pH 2.0, (b) pH 7.25, (c) pH 10.0 and (d) pH 12.0.

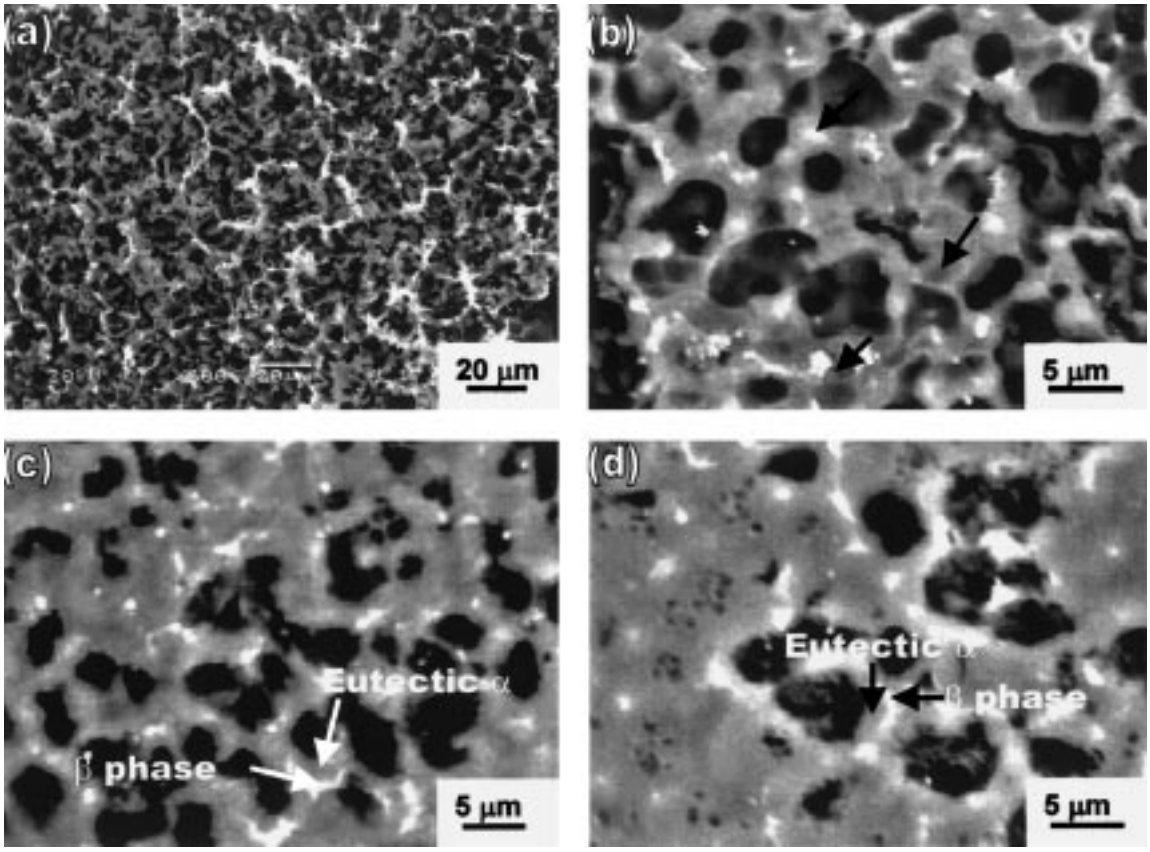

Fig. 10. Scanning electron micrographs for die-cast showing effect of pH on corrosion morphology: (a) pH 1.0, (b) pH 2.0, (c) pH 7.25 and (d) pH 12.0 (pictures (b), (c) and (d) are recorded in back scattered mode).

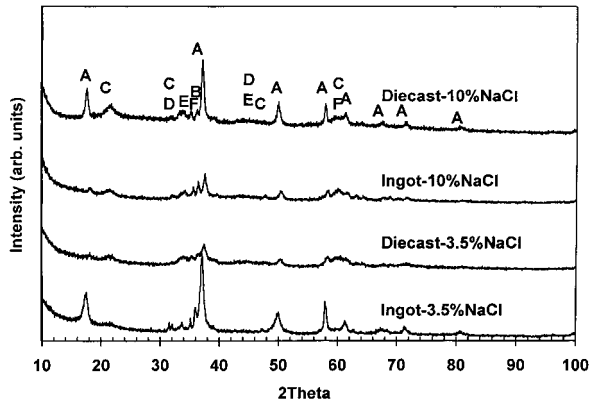

Fig. 11. XRD patterns of corrosion products for the materials in different chloride containing environments (A → $Mg(OH)_2$, B → β Phase, C → $MgAl_2(OH)_8$ xH_2O, D → $Mg_{0.866}Al_{1.83}O_{3.611}$, E → $Mg_2Al(OH)_{10}$ xH_2O, F → $MgAl(OH)_2$ xH_2O).

cathodic current densities. Under this condition (pH 12.0), for die-cast, the corrosion product consisted of (Figure 12) a considerable amount of magnesium–aluminium oxide, pointing to the fact that this might have contributed to the passivity. During immersion studies, the lowest corrosion rate was observed for die-cast under this condition (Figures 3 and 4), although electrochemical studies did not show significant difference from the value at pH 7.25.

In addition, the fine distribution of β phase in die-cast helps reducing the corrosion susceptibility. It has been

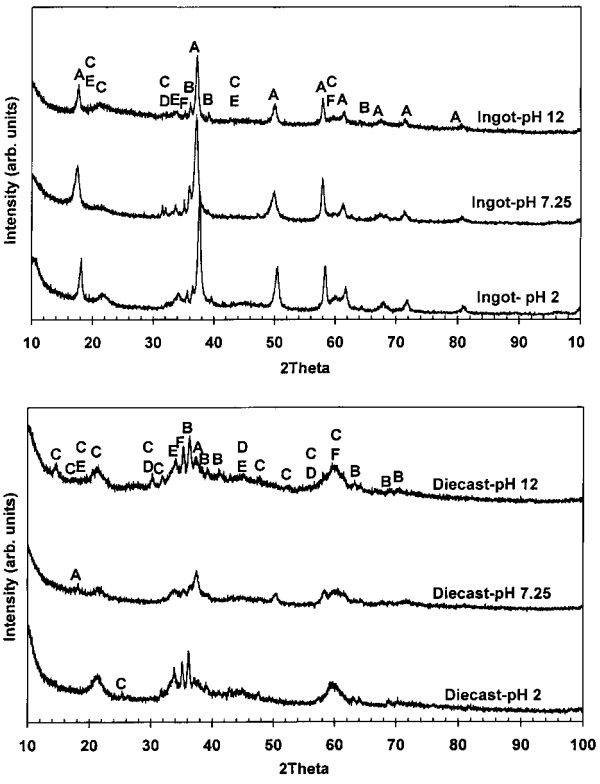

Fig. 12. XRD patterns of corrosion products for the materials under different pH conditions: (A → $Mg(OH)_2$, B → β phase, C → $MgAl_2(OH)_8$ xH_2O, D → $Mg_{0.866}Al_{1.83}O_{3.611}$, E → $Mg_2Al(OH)_{10}$ xH_2O, F → $MgAl(OH)_2$ xH_2O.

reported that [15] the β phase in AZ91 alloys could play dual role in dissolution behaviour depending on its morphology. It can act either as a galvanic cathode or a kinetic barrier to dissolution. If the α grains are fine and the β fraction is not too low, the oxide film formed on β phase is nearly continuous. On the one hand, in die-cast this was possible due to the close network of β phase (Figure 1); on the other hand, in ingot, the interparticle distance was very high so that such a networking was impossible.

The considerable difference in the corrosion rate obtained from immersion studies and electrochemical measurements may be attributed to the difference effect [14, 16–19] and to the physical removal of β phase during corrosion. Undermined β phases were found in the corrosion products, especially in aggressive solutions like pH 2.0, 12.0 and at 10% NaCl.

4.2. *Microcorrosion morphologies and corrosion products*

Surface morphology pictures in Figures 7–10 indicate that the corrosion behaviour of microconstituents was affected by the aggressiveness of the medium. In less aggressive media (e.g., at 3.5% NaCl and at pH 7.25) corrosion attack was concentrated primarily to regions with low concentration of aluminium (primary α). More aggressive solutions (10% NaCl and pH 2.0) spread the attack to otherwise stable eutectic α (regions with higher amount of aluminium) and to β phase. Figures 9 and 10 shows that at pH 2.0, the β phase was severely attacked and the corrosion product under this condition revealed evidence of higher aluminium containing compounds. The diffraction pattern of corrosion product also revealed higher amounts of fallen β phases, probably due to the severe corrosion at α/β interfaces. This may be due to the galvanic coupling between the eutectic α and β phase that is possible under this pH condition due to the absence of a protective film. At pH 12.0 for ingot a pitting type of attack was observed showing the presence of a protective film and in correlation with this the corrosion product showed mainly $Mg(OH)_2$. For die-cast at pH 12.0, a higher amount of fallen β phase and mixed oxide was seen in the product. This may be due to the corrosion of a very thin eutectic α phase in this material that led to undermining of the β phase. However, it is not clear why such a form of attack was not found on ingot; on the other hand the eutectic α and β phases were completely protected at this pH . Also, It is interesting to observe that, although undermining of the β phase occurred in die-cast under this condition, the corrosion rate at this pH at all chloride ion concentrations was much lower compared to that for ingot. As explained earlier this may be attributed to the presence mixed oxides together with the close network of β phase.

The presence of aluminium is reported to improve passivity in Mg–Al alloys. Lunder et al. [5] also reported that the composition of the film formed on Mg–Al alloy is pH dependent. It was either Mg rich or Al rich depending on the pH of the solution. Acidic (down to

pH 4.0) solution favoured Al oxide, while alkaline pH (upto 12.0) favoured Mg oxide. Makar and Kruger [20] reported that for Mg–Al alloys in sodium borate solution at pH 9.2 the oxide film on the Mg–Al alloy showed a layered structure composed of MgO/Mg–Al–oxide/ structure with the oxide (MgO) being thinner with increasing Al content.

5. Conclusions

(i) Increase in chloride ion concentration increased the corrosion rate of both ingot and die-cast at pH 7.25 and 12.0. At pH 2.0, the effect of chloride ion was found to be negligible. The effect of chloride ion was more significant for ingot. At pH 7.25, the OCP of both materials shifted to more negative (more active) values with increase in chloride concentration.

(ii) Both die-cast and ingot exhibited very high corrosion rate and more active OCP values in highly acidic solutions. The corrosion rate was found to be low in neutral pH and alkaline conditions.

(iii) The corrosion rate determined from immersion studies was much higher than that obtained from electrochemical measurements and, concurrent with this, corrosion product showed undermined β particles.

(iv) At higher chloride concentrations and aggressive pH conditions, otherwise stable β phase and eutectic α phases (i.e., α phase regions with aluminium content $>8\%$) were attacked and, correspondingly, the corrosion product showed a relatively higher amount of β particles and magnesium–aluminium oxide.

Acknowledgements

The authors thank Dr Qiu Jian Hai of NTU for his help in conducting the electrochemical experiments and Gintic Institute of Technology for providing the magnesium alloys. One of the authors (Zhou Wei) thanks Nanyang Technological University for a research grant RG79/98.

References

1. G.L. Makar and J. Kruger, *Int. Mat. Rev.* **38** (1993) 138.
2. I.J. Polmear, 'Light Alloys: Metallurgy of the Light Metals', 2nd edn. (Edward Arnold, New York, 1989), p. 183.
3. O. Lunder, T.Kr. Aune and K. Nisancioglu, *Corrosion* **43** (1987) 291.
4. D. Daloz, P. Steinmetz and G. Michot, *Corrosion* **53** (1997) 944.
5. O. Lunder, J.E. Lein, T.Kr. Aune and K. Nisancioglu, *Corrosion* **45** (1989) 741.
6. T. Beldjoudi, C. Fiaud and L. Robbiola, *Corrosion* **49** (1993) 738.
7. G.L. Makar, J. Kruger and K. Sieradzki, *J. Electrochem. Soc.* **139** (1992) 47.
8 Annual Book of ASTM Standards, Parts 3 and 4 (1977) 722.
9. R. Ambat, N.N. Aung and W. Zhou, *Corros. Sci.* (1999) in press.
10. H. Bommer, *in* B.L. Mordike and K.U. Kainen (Eds), 'Magnesium Alloys and Their Applications', Proceedings of the Conference on 'Magnesium Alloys and Their Applications', (Werkstoff-infomationsgesellschaft, 1998), p. 79.
11. A. Frumkin, *in* E. Yeager (Ed.), Transactions of the Symposium on 'Electrode Process', The Electrochemical Society, New York, 4–6 May, 1959 (J. Wiley & Sons, New York, 1961), p. 1.
12. M. Pourbaix, 'Atlas of Electrochemical Equilibrium Diagrams in Aqueous Solutions' (NACE, Houston, TX, 1966).
13. H.H. Uhlig and R. Winston Revie, 'Corrosion and Corrosion Control' (New York, J. Wiley and Sons, 1985), chapter 20.
14. C.H. Brun, J. Pagetti and J. Talbot, *Mem. Sci. Rev. Metall.* **73** (1976) 659.
15. G. Song, A. Atrens and M. Dargusch, *Corros. Sci.* **41** (1999) 249.
16. G. Song, A. Atrens, D. Stjohn, J. Nairn and Y. Li, *Corrosi. Sci.* **39** (1997) 855.
17. R.L. Petty, W. Davidson and J. Kleinberg, *J. Am. Chem. Soc.* **76** (1954) 363.
18. J.H. Greenblatt, *J. Electrochem. Soc.* **103** (1956) 539.
19. J.H. Greenblatt, *Can. J. Chem.* **36** (1958) 1138.
20. G.L. Makar and J. Kruger, *J. Electrochem. Soc.* **137** (1990) 414.